



This is a repository copy of *Algorithm for transient growth of perturbations in channel Poiseuille flow*.

White Rose Research Online URL for this paper:
<https://eprints.whiterose.ac.uk/207833/>

Version: Accepted Version

Article:

Zhang, J., Dong, G. and Li, Y. orcid.org/0000-0001-7907-5176 (2017) Algorithm for transient growth of perturbations in channel Poiseuille flow. *Applied Mathematics and Mechanics*, 38 (11). pp. 1635-1650. ISSN 0253-4827

<https://doi.org/10.1007/s10483-017-2275-9>

This version of the article has been accepted for publication, after peer review (when applicable) and is subject to Springer Nature's AM terms of use, but is not the Version of Record and does not reflect post-acceptance improvements, or any corrections. The Version of Record is available online at: <http://dx.doi.org/10.1007/s10483-017-2275-9>.

Reuse

Items deposited in White Rose Research Online are protected by copyright, with all rights reserved unless indicated otherwise. They may be downloaded and/or printed for private study, or other acts as permitted by national copyright laws. The publisher or other rights holders may allow further reproduction and re-use of the full text version. This is indicated by the licence information on the White Rose Research Online record for the item.

Takedown

If you consider content in White Rose Research Online to be in breach of UK law, please notify us by emailing eprints@whiterose.ac.uk including the URL of the record and the reason for the withdrawal request.



eprints@whiterose.ac.uk
<https://eprints.whiterose.ac.uk/>

Submission to Applied Mathematics and Mechanics

**An algorithm for transient growth of perturbations in channel
Poiseuille flow**

Jianlei ZHANG¹, Gang DONG^{1,†}, Yi LI²

1. National Key Laboratory of Transient Physics, Nanjing University
of Science and Technology, Nanjing 210094, China;
2. School of Mathematics and Statistics, University of Sheffield,
Sheffield S3 7RH, U.K.

† Corresponding author's contact information

Prof. Gang Dong (Ph. D.)

National Key Laboratory of Transient Physics,
Nanjing University of Science and Technology,
Nanjing, Jiangsu 210094, China,

Tel: +86-25-84303236

Fax: +86-25-84315644

Email address: dgvehicle@yahoo.com

Abstract This study develops a direct optimal growth algorithm for three-dimensional transient growth analysis of perturbations in channel flows which are globally stable but locally unstable. Different from the traditional non-modal method which is based on the Orr-Sommerfeld and Squire (OSS) equations that assume simple base flows, this algorithm can be applied to arbitrarily complex base flows. In this **algorithm**, a re-orthogonalization Arnoldi method is employed to improve the orthogonality of the orthogonal basis of the Krylov subspace generated by **solving** linearized forward and adjoint Navier-Stokes (NS) equations. The linearized adjoint Navier-Stokes equations with specific boundary conditions of the channel are deduced, and a new convergence criterion is proposed. The algorithm is then applied to the plane Poiseuille flow **in a channel**. The effects of spanwise width of the channel and Reynolds number on the transient growth of perturbations are studied. The results show that optimal flow field leading to the largest growth of perturbations is characterized by high- and low-speed streaks and the corresponding streamwise vortical structures. The algorithm is validated by comparing the results obtained from the OSS equations method. A lift-up mechanism that induces the transient growth of perturbations is discussed.

Key words transient growth, Poiseuille flow, Arnoldi method, Krylov subspace, adjoint equations

Chinese Library Classification O357.4+1

2010 Mathematics Subject Classification 35E15, 34D30

1 Introduction

Linear stability theory is concerned with whether a laminar base flow changes its state when perturbations with infinitesimal amplitude are added. If the state changes, then the base flow is unstable. If the base flow returns to the original state, then it is stable. To date, several numerical methods have been developed successfully for linear stability analysis, e.g. modal stability analysis, non-modal stability analysis and the so-called direct optimal growth analysis.

Traditionally, the linear stability of a flow has been analyzed using the modal approach. In this approach, the asymptotic behavior of small perturbations to a steady or time-periodic base flow is **usually** considered. This behavior is determined by the eigenvalues of the linear operator derived from the linearized Navier-Stokes (**NS**) equations, because the eigenvalues characterize the evolution of the perturbations. For some flows, especially for those with instability driven by thermal or centrifugal forces, e.g., Rayleigh-Bénard convection and Taylor-Couette flow, the predictions of modal analysis agree well with laboratory experiments^[1, 2].

Despite remarkable accomplishments of the modal analysis, many questions are left unanswered. For example, discrepancy exists between the computed critical Reynolds number and the observed ones in many wall-bounded shear flows, and the theoretically predicted structures are not always observed in unforced experiments^[3]. The drawback of this modal approach is associated with the non-orthogonality of the eigenmodes of the linearized flow system. As a consequence, non-modal analysis theories^[4] are needed for many problems. This theory, referred to here as the transient

growth theory, emphasizes the linear nature of the non-modal amplification mechanism and is based on the observation that an initial perturbation that is not a pure eigenmode may undergo transient growth, even though all eigenmodes decay monotonically. This transient growth may lead to nonlinear instability or otherwise change the path of instability, leading to, e.g., bypass transition to turbulence. Among this form of initial perturbations, the one which yields the largest amplification is referred to as being “optimal”.

If the evolution of the perturbations are governed by the Orr-Sommerfeld and Squire (OSS) equations^[5], it is possible to directly evaluate the eigenvalues of the operator matrix. However, it is difficult, and in some cases impossible, to build the operator matrix for general complex base flows. Therefore, a direct optimal growth method (also called matrix-free method) for both modal and non-modal instability was recently presented by Barkley et al.^[6] Because this method is suitable for stability analysis of flows with arbitrary complexity, it has been applied in stability analysis of various flows, e.g., flow over a backward-facing step^[7], stenotic flows^[8-10], flow past a circular cylinder^[11, 12], vortex pair systems^[13], flow through a sudden expansion in a circular pipe^[14] and flow over a turbine blade^[15]. In this method, a Krylov subspace can be constructed to approximate the eigenmodes of large matrix by explicitly solving the linearized NS equations and their adjoints by iterations. This method, however, depends on the specific boundary conditions of the flow. Thus, the linearized adjoint Navier-Stokes equations should be determined if it is applied to base flows with other boundary conditions.

In this paper, we improve the direct optimal growth method and apply it to the plane Poiseuille flow in a channel, which has been not addressed before. A detailed derivation of linearized adjoint NS equations of the channel flow with specific boundary conditions is presented, and the direct numerical simulation (DNS) based on the spectral method is then used to solve the linearized NS equations and corresponding adjoint ones. The algorithm based on the Krylov subspace, which approximates the perturbation growth is reformed by using a re-orthogonalization Arnoldi technology in order to improve the orthogonality of the orthogonal basis of the Krylov subspace. The improved algorithm is then combined with the DNS method to fit the temporally developed global instability in such flow. Based on the algorithmic strategy, the effects of Reynolds number and spanwise width of the channel on the transient growth of perturbations are investigated. A mechanism that induces transient growth of perturbations in channel flow is discussed.

2 Numerical method

2.1 Transient growth of infinitesimal perturbations

Considering a general incompressible flow \mathbf{U} in a three-dimensional domain (Ω), the linearized NS equations of infinitesimal perturbations can be expressed as:

$$\partial_t \mathbf{u} = -(\mathbf{U} \cdot \nabla) \mathbf{u} - (\mathbf{u} \cdot \nabla) \mathbf{U} - \nabla p + \nu \nabla^2 \mathbf{u} \quad \text{with} \quad \nabla \cdot \mathbf{u} = 0 \quad \text{in } \Omega \quad (1)$$

Here \mathbf{u} and p are the infinitesimal perturbation velocity and kinematic pressure, respectively; ν is the fluid viscosity defined by $\nu = Q/\text{Re}$, where Q is the constant-volume-flow rate, Re is the bulk Reynolds number; \mathbf{U} is the base flow. In this study, we choose the laminar plane Poiseuille flow solution as \mathbf{U} , whose

non-dimensional profile is given by

$$(2) \quad U(y) = 1 - y^2$$

where y is the coordinate in the direction normal to the channel walls and $y \in [-1, 1]$.

The linear evolution of a perturbation from $t = 0$ to a later time t under Eq. (1) can be expressed concisely as the action of a linear evolution operator $\mathbf{A}(t)$ on the initial perturbation $\mathbf{u}(\mathbf{x}, 0)$:

$$\mathbf{u}(\mathbf{x}, t) = \mathbf{A}(t)\mathbf{u}(\mathbf{x}, 0) \quad (3)$$

Usually, the modal analysis focuses on the asymptotic behavior of the perturbations, which is characterized by the eigenvalues of the system and the evolution of the eigenmodes. However, owing to the non-orthogonality of the eigenmodes of the linearized NS equations, the dynamics of interest may not be of the form of an exponential function of time multiplying a fixed modal shape, therefore, the eigenvalue problem in modal analysis is not directly relevant^[2,5]. Thus, a transient growth method is preferred to quantify such dynamics, which is concerned with the maximum energy growth for all possible initial perturbations over a finite time interval.

Typically, the total kinetic energy, E , of a perturbation field over the full flow domain is chosen to quantify the size of the perturbations^[5], derived from the L_2 inner product of the perturbed velocity, \mathbf{u} :

$$E = \frac{1}{2}(\mathbf{u}, \mathbf{u}) \equiv \frac{1}{2} \int_{\Omega} \mathbf{u} \cdot \mathbf{u} d^3x \quad (4)$$

here (\cdot, \cdot) is the standard L_2 inner product in space. Transient growth is described by the growth of the energy norm of the perturbations over a given time interval, and can

be quantitatively measured by the ratio of final energy at time t to initial energy at time 0. Setting the norm of the initial perturbations to unit, i.e., $\|\mathbf{u}(0)\|=1$, the transient energy growth over interval t is:

$$\begin{aligned} \frac{E(t)}{E(0)} &= \|\mathbf{u}(t)\|^2 = (\mathbf{u}(t), \mathbf{u}(t)) = (\mathbf{A}(t)\mathbf{u}(0), \mathbf{A}(t)\mathbf{u}(0)) \\ &= (\mathbf{u}(0), \mathbf{A}^*(t)\mathbf{A}(t)\mathbf{u}(0)) \end{aligned} \quad (5)$$

where, $\mathbf{A}^*(t)$ is the adjoint evolution operator of $\mathbf{A}(t)$.

The goal of transient growth analysis is to find the maximum energy growth and the corresponding initial perturbations, i.e., the optimal growth and the optimal perturbations. From Eq. (5), it is obvious that seeking the optimal growth is equivalent to finding the leading eigenvalue of operator $\mathbf{A}^*(t)\mathbf{A}(t)$, and the corresponding eigenmode is the optimal perturbation. Let λ_j and \mathbf{v}_j denote an eigenvalue and the corresponding normalized eigenmode of $\mathbf{A}^*(t)\mathbf{A}(t)$, respectively, we have

$$\mathbf{A}^*(t)\mathbf{A}(t)\mathbf{v}_j = \lambda_j\mathbf{v}_j, \quad \|\mathbf{v}_j\|=1 \quad (6)$$

Thus, the maximum energy growth at time t , denoted as $G(t)$, can be derived as

$$G(t) \equiv \max_{\|\mathbf{u}^*(0)\|=1} \frac{E(t)}{E(0)} = \max_j \lambda_j = \lambda_{\max} \quad (7)$$

2.2 Linearized adjoint NS equations

$\mathbf{A}^*(t)$ in Eq. (5) represents the evolution operator for the linearized adjoint equations of perturbations with the same boundary conditions as the linearized equations. In this section, we derive the linearized adjoint NS equations with the specific boundary conditions for channel flow.

The linearized adjoint NS equations can be divided into three parts, that is, the advection term, the viscous and pressure term, and the time derivative term. Let \mathbf{H} be an operator representing one of these three terms, then \mathbf{H} and its adjoint operator

\mathbf{H}^* must satisfy the following relation based on the L_2 inner product in the domain of space Ω and time $[0, \tau]$:

$$(\mathbf{u}^*, \mathbf{H}(\mathbf{u})) = (\mathbf{u}, \mathbf{H}^*(\mathbf{u}^*))$$

(8)

for arbitrary functions \mathbf{u} and \mathbf{u}^* with homogeneous boundary conditions in the wall normal direction and periodic boundary conditions in the streamwise and spanwise directions.

For the advection term, we define advection operator \mathbf{DN} as:

$$\mathbf{DN}(\mathbf{u}) = (U_j \partial_j \mathbf{u}) + (\partial_j U_j) \mathbf{u} \quad (9a)$$

or

$$(\mathbf{DN}\mathbf{u})|_i = U_j \partial_j u_i + (\partial_j U_j) u_j \quad (9b)$$

According to the definition of inner product in Eq. (4), one obtains

$$\begin{aligned} (\mathbf{u}^*, \mathbf{DN}(\mathbf{u})) &= \int_{\Omega} \mathbf{u}^* \cdot \mathbf{DN}(\mathbf{u}) d^3x = \int_{\Omega} u_i^* U_j \partial_j u_i d^3x + \int_{\Omega} (u_i^* \partial_j U_j) u_j d^3x \\ &= \oint_{\partial\Omega} u_i^* U_j u_i \hat{n}_j dS - \int_{\Omega} [\partial_j (u_i^* U_j)] u_i d^3x + \int_{\Omega} (u_i^* \partial_j U_j) u_j d^3x \\ &= - \int_{\Omega} [\partial_j (u_i^* U_j)] u_i d^3x + \int_{\Omega} (u_i^* \partial_j U_j) u_j d^3x \\ &= \int_{\Omega} [-U_j \partial_j u_i^* + u_j^* \partial_j U_j] u_i d^3x = (\mathbf{DN}^*(\mathbf{u}^*), \mathbf{u}) \end{aligned} \quad (10)$$

The boundary conditions in the **channel flow** presented in this study are such that perturbations on the no-slip wall are zero and are periodic in the streamwise (x) and spanwise (z) directions. Thus, the surface integral $\oint_{\partial\Omega} u_i^* U_j u_i \hat{n}_j dS$ in Eq. (10) is zero, and the adjoint advection operator \mathbf{DN}^* can be expressed as follows according to Eq. (8),

$$\mathbf{DN}^* \mathbf{u}^*|_i = -U_j \partial_j u_i^* + u_j^* \partial_j U_j \quad (11a)$$

or

$$\mathbf{DN}^* \mathbf{u}^* = -(\mathbf{U} \cdot \nabla) \mathbf{u}^* + (\nabla \mathbf{u}^*)^T \cdot \mathbf{u}^* \quad (11b)$$

The viscous and pressure terms in Eq. (1), as well as the continuity equation, are all linear hence can be treated together. These terms can be written as

$$\begin{bmatrix} \nu \nabla^2 & -\nabla \\ \nabla \cdot & 0 \end{bmatrix} \begin{bmatrix} \mathbf{u} \\ p \end{bmatrix} \quad (12)$$

According to the definition of inner product in Eq. (4), we have

$$\begin{aligned} & \left(\begin{bmatrix} \nu \nabla^2 & -\nabla \\ \nabla \cdot & 0 \end{bmatrix} \begin{bmatrix} \mathbf{u} \\ p \end{bmatrix}, \begin{bmatrix} \mathbf{u}^* \\ p^* \end{bmatrix} \right) \\ &= \int_{\Omega} [(\nu \nabla^2 \mathbf{u} - \nabla p) \cdot \mathbf{u}^* + (\nabla \cdot \mathbf{u}) p^*] d^3x \\ &= \int_{\Omega} \left\{ \nu [\partial_k (u_i^* \partial_k u_i) - \partial_k u_i^* \partial_k u_i] - \nabla \cdot (p \mathbf{u}^*) + p \nabla \cdot \mathbf{u}^* + \nabla \cdot (p^* \mathbf{u}) - \mathbf{u} \cdot \nabla p^* \right\} d^3x \quad (13) \\ &= \int_{\Omega} \left\{ \nu [-\partial_k u_i^* \partial_k u_i] + p \nabla \cdot \mathbf{u}^* - \mathbf{u} \cdot \nabla p^* \right\} d^3x \\ &= \int_{\Omega} \left\{ \nu [-\partial_k (u_i \partial_k u_i^*) + u_i \partial_k^2 u_i^*] + p \nabla \cdot \mathbf{u}^* - \mathbf{u} \cdot \nabla p^* \right\} d^3x \end{aligned}$$

Note that $\int_{\Omega} \nu \partial_k (u_i^* \partial_k u_i) d^3x = 0$, $\int_{\Omega} \nu [-\partial_k (u_i \partial_k u_i^*)] d^3x = 0$, $\int_{\Omega} \nabla \cdot (p \mathbf{u}^*) d^3x = 0$ and

$\int_{\Omega} \nabla \cdot (p^* \mathbf{u}) d^3x = 0$ in Eq. (13), by the divergence theorem and the boundary conditions.

Thus, Eq. (13) can be rewritten as follows,

$$\begin{aligned} \left(\begin{bmatrix} \nu \nabla^2 & -\nabla \\ \nabla \cdot & 0 \end{bmatrix} \begin{bmatrix} \mathbf{u} \\ p \end{bmatrix}, \begin{bmatrix} \mathbf{u}^* \\ p^* \end{bmatrix} \right) &= \int_{\Omega} [\nu (\nabla^2 \mathbf{u}^*) \cdot \mathbf{u} - (\nabla p^*) \cdot \mathbf{u} + (\nabla \cdot \mathbf{u}^*) p] d^3x \\ &= \left(\begin{bmatrix} \nu \nabla^2 & -\nabla \\ \nabla \cdot & 0 \end{bmatrix} \begin{bmatrix} \mathbf{u}^* \\ p^* \end{bmatrix}, \begin{bmatrix} \mathbf{u} \\ p \end{bmatrix} \right) \quad (14) \end{aligned}$$

From Eqs. (8) and (14), we can see that the adjoint operator of the coupled linear operator is the same as itself; that is, this operator is self-adjoint.

The adjoint operator of the time derivative term in Eq. (1) can be deduced as

follows,

$$\begin{aligned}
 (\mathbf{u}^*, \partial_t \mathbf{u}) &= \int_0^\tau \int_\Omega \mathbf{u}^* \cdot \partial_t \mathbf{u} d^3x dt \\
 &= \int_\Omega [\mathbf{u} \cdot \mathbf{u}^*]_0^\tau d^3x - \int_0^\tau \int_\Omega \mathbf{u} \cdot \partial_t \mathbf{u}^* d^3x dt
 \end{aligned} \quad (15)$$

Equation (15) shows that the adjoint of the time derivative term is $-\partial_t \mathbf{u}^*$.

According to Eqs. (11), (14) and (15), the adjoint of the linearized NS equations for infinitesimal perturbations are written as

$$-\partial_t \mathbf{u}^* = (\mathbf{U} \cdot \nabla) \mathbf{u}^* - (\nabla \mathbf{U})^T \cdot \mathbf{u}^* - \nabla p^* + \nu \nabla^2 \mathbf{u}^* \quad \text{with } \nabla \cdot \mathbf{u}^* = 0 \quad \text{in } \Omega \quad (16)$$

2.3 Algorithm of direct optimal growth

Equation (6) indicates that the main purpose of the transient growth is searching for the leading eigenvalue (λ_{max}) of the combined operator $\mathbf{A}^*(t)\mathbf{A}(t)$ and the corresponding eigenvector. In the direct optimal growth method, a Krylov subspace $\{\mathbf{u}_0, \mathbf{M}\mathbf{u}_0, \mathbf{M}^2\mathbf{u}_0, \dots, \mathbf{M}^k\mathbf{u}_0\}$ is first constructed by acting the operator \mathbf{M} for initial vector \mathbf{u}_0 repeatedly, here operator \mathbf{M} represents $\mathbf{A}^*(t)\mathbf{A}(t)$. That is, the Krylov subspace can be obtained from the repeatedly integrating the linearized forward and subsequent adjoint NS equations for \mathbf{u}_0 . Subsequently, a standard QR decomposition is employed to obtain the orthogonal basis of the Krylov subspace, which is used to obtain the eigenmode information of the linearized system. However, it is sometimes ill-suited to construct the orthogonal basis of the Krylov subspace by the standard QR decomposition. Because sometimes the application of the Krylov subspace on specific flows are ill conditioned and the orthogonality of the orthogonal basis of the Krylov subspace is getting worse along with construction process of the Krylov space. Actually, it is the orthogonal basis of the Krylov subspace, not the Krylov subspace

itself, that is used in applications. Thus, it is preferred to use the classical Arnoldi technique^[16] to improve the orthogonality, which does not construct the Krylov subspace but directly calculates the orthogonal basis of it by the standard QR decomposition. In addition, to further improve the orthogonality of the orthogonal basis, a re-orthogonalization technique can also be employed on the basis of the classical Arnoldi method.

Figure 1 gives the orthogonality of the orthogonal basis of the Krylov subspace for present study, here the orthogonality used in the figure is defined as $\|\mathbf{Q}^T\mathbf{Q}-\mathbf{I}\|_2$, in which \mathbf{I} is unit matrix, and \mathbf{Q} is the orthogonal basis which is derived by standard QR decomposition of Krylov subspace (method I), the classical Arnoldi technique (method II) and the re-orthogonalization Arnoldi technique (method III), respectively. It can be seen that the orthogonality by the method I is getting much worse than the other two methods with iteration. And the orthogonality by the method III is slightly better than that by the method II.

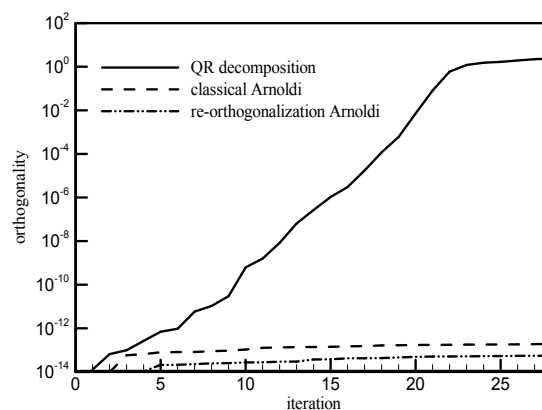


Fig. 1 Orthogonality with iteration by different methods for a plane Poiseuille flow in the channel. The spanwise width of the channel is π , $Re=2670$ and $t=10$.

We now give the procedure for the algorithm of direct optimal growth based on the re-orthogonalization Arnoldi technique to compute the leading eigenvalue (i.e., the maximum growth) and the corresponding eigenvector (i.e., the optimal initial

perturbation) of the linearized channel flow.

Define a set of orthogonal basis of a k -dimensional Krylov subspace as:

$$\mathbf{Q}_k \equiv \text{span}\{\mathbf{q}_0, \mathbf{q}_1, \dots, \mathbf{q}_{k-1}\} \quad (17)$$

(i) Initialize: Provide a positive integer $kmax$ as the maximum dimension of \mathbf{Q}_k in Eq. (17), a residual norm tolerance tol (which is the measurement of convergence in iterations) and an initial vector \mathbf{q}_0 with unit norm. Set $k=0$.

(ii) Integrate linearized forward and adjoint NS equations (Eqs. (1) and (16)), taking \mathbf{q}_k as the initial perturbation:

for (int $k = 0; k < kmax; k++$) {

$$\mathbf{w} = \mathbf{A}^* \mathbf{A} \mathbf{q}_k;$$

(iii) Perform orthogonalization procedure of classical Arnoldi method by using a modified Gram-Schmidt approach:

for (int $i = 0; i \leq k; i++$) {

$$h_{ik} = \mathbf{q}_i^T \mathbf{w};$$

$$\mathbf{w} = \mathbf{w} - h_{ik} \mathbf{q}_i;$$

}

(iv) Perform the re-orthogonalization procedure to improve the orthogonality of orthogonal basis of the Krylov subspace:

for (int $i = 0; i \leq k; i++$) {

$$s = \mathbf{q}_i^T \mathbf{w};$$

$$h_{ik} = h_{ik} + s;$$

$$\mathbf{w} = \mathbf{w} - h_{ik} \mathbf{q}_i;$$

}

(v) Calculate the leading eigenvalue λ_{max} and the corresponding eigenvector \mathbf{v}_{max} of \mathbf{H} , which consists of h_{ik} from step (iv). In other words, h_{ik} is the element of \mathbf{H} .

Compute the Ritz eigenvector $\mathbf{Q}_k \mathbf{v}_{\max}$. Calculate $h_{k+1,k}$ and the residential norm rn as :

$$h_{k+1,k} = \|\mathbf{w}\|_2;$$

$$\text{if } k > 0 \text{ then } rn = \|\lambda_{\max}^{(k)} - \lambda_{\max}^{(k-1)}\|_2;$$

where $\lambda_{\max}^{(k)}$ and $\lambda_{\max}^{(k-1)}$ are the leading eigenvalues in k -th and $(k-1)$ -th iterations, respectively.

if $rn > tol$, calculate $\mathbf{q}_{k+1} = \mathbf{w}/h_{k+1,k}$ and goto step(ii).

} The program ends.

In step (ii), we use the **DNS** based on the standard Fourier-Chebyshev spectral method^[17] to integrate the linearized forward and adjoint NS equations. In this simulation, the Chebyshev- τ method and the no-slip condition are used in the non-homogeneous wall-normal direction (y -direction), while Fourier expansion is used in the homogeneous directions, i.e., the streamwise (x) and spanwise (z) directions of the channel. A Chebyshev- τ influence-matrix method, including a τ -correction step, is employed for the viscous and pressure term to ensure that the computed solutions satisfy both the incompressibility constraint and the momentum equation. The aliasing errors in the x - and z -directions are removed by truncation according to the 3/2-rule. The time advancement is carried out by using a semi-implicit backward-difference scheme with third-order accuracy. This numerical method has been well tested in our previous studies^[18, 19].

Note that the magnitude of $h_{k+1,k}$ is used to judge the convergence of the iterations in [6]. However, the convergence of $h_{k+1,k}$ is not necessary in this study since we are focusing on the optimal growth. Therefore, we take $rn = \|\lambda_{\max}^{(k)} - \lambda_{\max}^{(k-1)}\|_2$ as the measure of convergence in our computations, and discuss the validity in section

3.3. In this study, we set $tol=1\times 10^{-4}$. Usually convergence can be obtained in about 6-13 iterations.

3 Results and discussions

In this paper, we investigate the transient growth of perturbations of plane Poiseuille flow in the channel. Note that, in this case, the base flow is in parallel to the homogenous streamwise direction (see. Eq. (2)). However, the algorithm presented in this work is applicable to any complex base flows in a channel, i.e., there is no limitation on the form of \mathbf{U} in Eqs. (1) and (16). The reason to choose the Poiseuille-type base flow in this work is twofold. Firstly, we intend to validate the algorithm by the OSS method. Secondly, the effects of the spanwise width (L_z) and Reynolds number (Re) of the channel flow on the transient growth of perturbations are investigated. The channel box, i.e., the computational domain, has a fixed streamwise length of $L_x=\pi$, and a fixed wall-normal height of $L_y=2$ (ranged from -1 to 1), and variable spanwise width L_z . Table 1 gives the computational cases with the different values of L_z and Re.

Table 1 Computational cases

cases	Re=2670		cases	Re=1000	
	L_z	$n_x \times n_y \times n_z^a$		L_z	$n_x \times n_y \times n_z$
1	$8/3\pi$	$32 \times 33 \times 192$	10	$12/5\pi$	$32 \times 33 \times 64$
2	$4/3\pi$	$32 \times 33 \times 64$	11	2π	$32 \times 33 \times 32$
3	$7/6\pi$	$32 \times 33 \times 64$	12	$8/5\pi$	$32 \times 33 \times 32$
4	π	$32 \times 33 \times 64$	13	$6/5\pi$	$32 \times 33 \times 32$
5	$5/6\pi$	$32 \times 33 \times 64$	14	π	$32 \times 33 \times 32$
6	$2/3\pi$	$32 \times 33 \times 32$	15	$4/5\pi$	$32 \times 33 \times 32$
7	$7/12\pi$	$32 \times 33 \times 32$	16	$3/5\pi$	$32 \times 33 \times 32$
8	$1/2\pi$	$32 \times 33 \times 32$	17	$2/5\pi$	$32 \times 33 \times 32$
9	$1/3\pi$	$32 \times 33 \times 32$			

^a n_x and n_y and n_z are the grid points in x , y and z directions, respectively.

3.1 Effects of L_z and Re on transient growth

Figure 2 firstly gives the profiles of transient growth (optimal growth), $G(t)$, of perturbations at different L_z for $Re=2670$. One can see that, in all cases, $G(t)$ increases with time until it reaches the maximum value (defined as G_{\max}), and then decreases. Besides, Fig. 2(a) shows that the maximum growth G_{\max} in each case increases with spanwise width L_z for L_z between $1/3\pi$ and π . Beyond $L_z > \pi$, G_{\max} no longer increases, as is shown in Fig. 2(b). Figure 3 gives the variations of $G(t)$ for various spanwise widths at $Re=1000$. The profiles of $G(t)$ and corresponding G_{\max} for $Re=1000$ show the similar behavior with those at $Re=2670$.

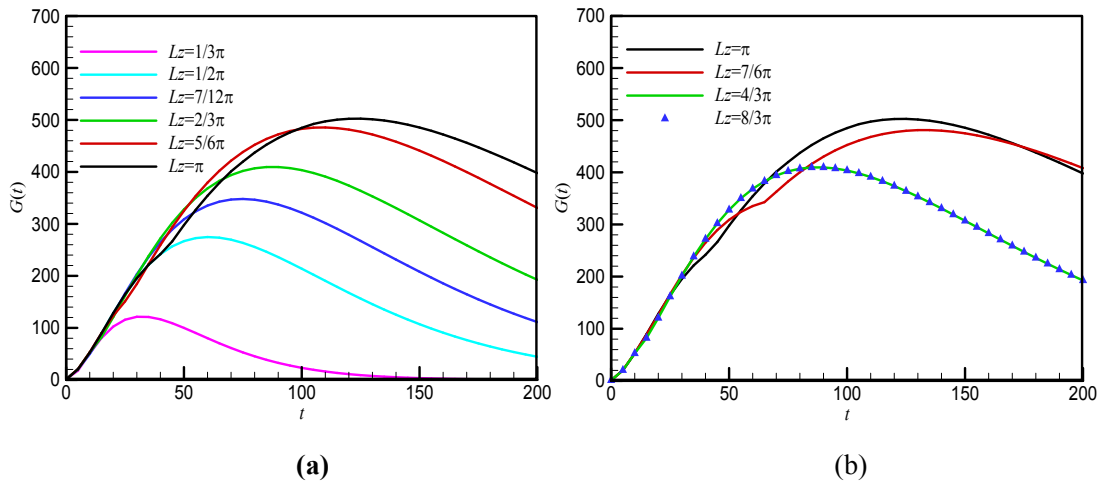


Fig. 2 Transient growth at different spanwise widths for $Re=2670$.

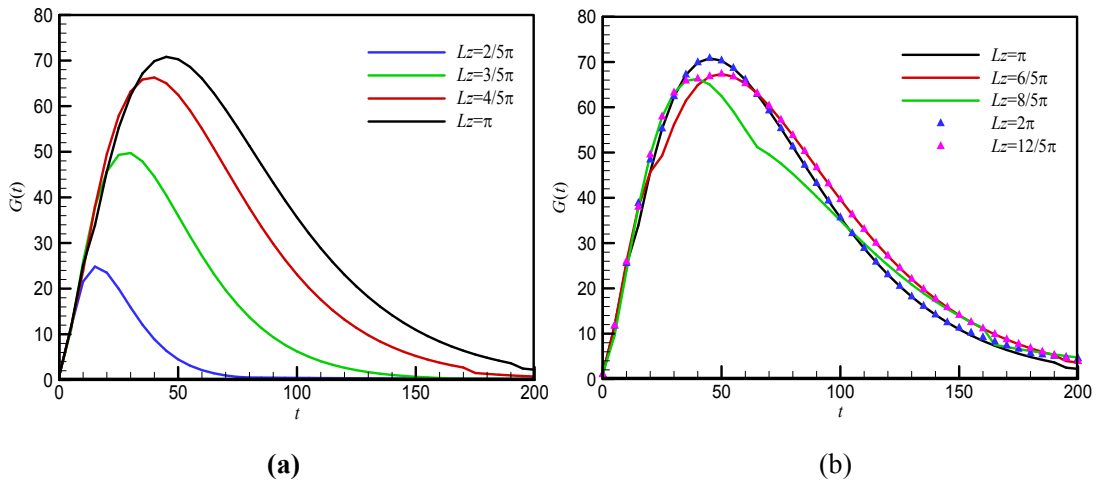


Fig. 3 Transient growth at different spanwise widths for $Re=1000$.

Figure 4 further depicts the variations of the maximum growth, G_{\max} , with the spanwise width for both Re numbers. It is clear that G_{\max} increases at small L_z until it reaches its largest value at $L_z=\pi$ and then fluctuates and eventually tends to a constant. In addition, G_{\max} shows similar behaviors for both Re numbers, except that the value of maximum growth for Re=1000 is smaller than that for Re=2670 at the same spanwise width. Figure 5 plots t_{\max} vs G_{\max} for the two Re numbers, where t_{\max} is defined as the time when $G(t)$ reaches G_{\max} . One can see the good linear relationship between t_{\max} and G_{\max} . This relationship implies that the variations of t_{\max} along with L_z is similar to G_{\max} vs L_z in Fig.4.

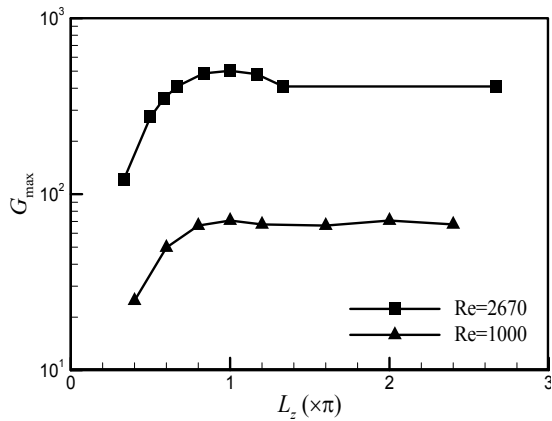


Fig. 4 Maximum growth vs spanwise width for Re=1000 and Re=2670.

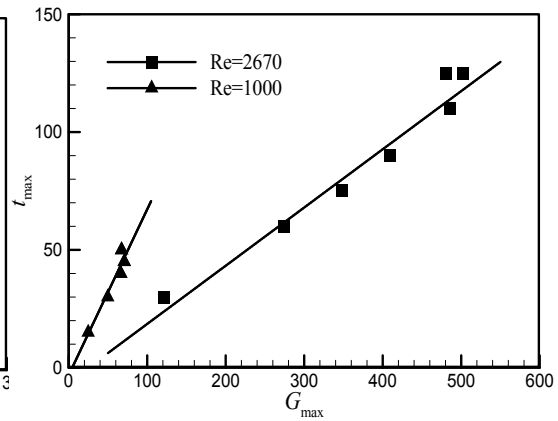


Fig. 5 Maximum time vs maximum growth for Re=1000 and Re=2670.

To understand the dependence of G_{\max} on L_z , we choose three typical spanwise widths of the computational box to inspect the optimal streamwise velocity perturbation, u , at t_{\max} for Re=1000, as is shown in Fig.6. Note that the structures of the optimal perturbation field are x -independent, therefore only structures in y - z section are shown. It can be seen that the alternating low speed and high speed regions in z direction are observed. In addition, such alternating regions occur both in the upper and bottom parts of the channel with **half** phase-shift in z direction. The high

and low speed regions actually represent the high-speed and low-speed streaks in optimal flow field. The occurrence of these streaks implies that the most dangerous state to destabilize the flow is the streaky structure which has been observed in transitional and developed boundary layer flows^[20]. Due to periodicity in z direction, the streaks always appear in pairs (one low-speed streak and one high-speed streak). Smaller spanwise width leads to narrower spacing between the low and high speed streaks (Fig. 6(a)), whereas for spanwise width $L_z=\pi$ the spacing between the streaks is optimal and the appropriate shape of the streaks is shown (Fig. 6(b)). When the spanwise width of the computational box is further extended to 2π (Fig. 6(c)), the shape and the spacing of the streak remain the same as those in the case with spanwise width π . These results indicate that π is the critical size to attain the maximum growth of the perturbations, as also shown in Fig. 4.

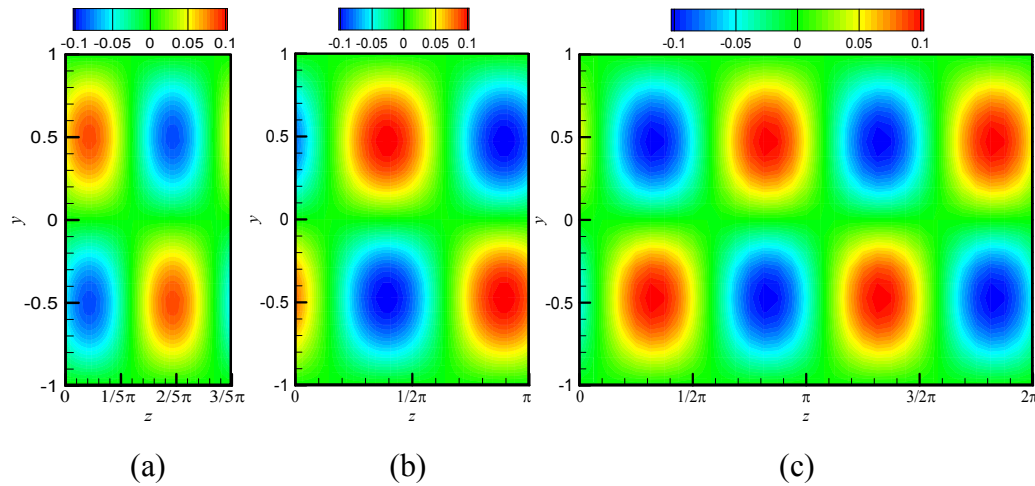


Fig. 6 Optimal perturbations for $Re=1000$. (a) $L_z=3/5\pi$, $t_{\max}=30$; (b) $L_z=\pi$, $t_{\max}=45$; (c) $L_z=2\pi$, $t_{\max}=45$.

The results of Fig. 4 also show that the critical size π is independent on the Reynolds number. Considering the wavelike solution of the perturbations in z direction, that is, $\mathbf{u}=\hat{\mathbf{u}}e^{i(\beta z)}$, where β is the spanwise wave number, we have

$$\beta = 2 \quad \pi \quad /L_z$$

(18)

Thus, we can explore the variations of G_{\max}/Re^2 along with β , as shown in Fig.7. It is obvious that the curves overlap for both $Re=2670$ and $Re=1000$ and that G_{\max}/Re^2 reaches the peak when $\beta=2$. In other words, the maximum growths reach peak at $\beta=2$

regardless of variations of Re number.

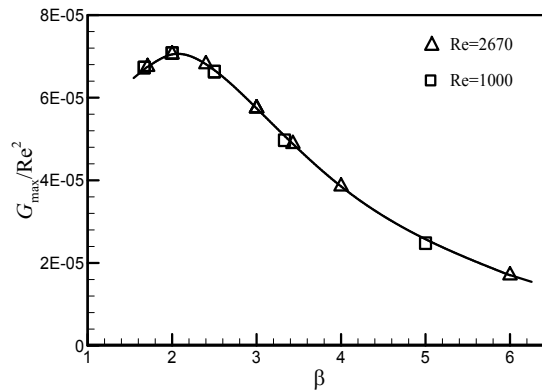


Fig. 7 G_{\max}/Re^2 with spanwise wave number for $Re=1000$ and $Re=2670$.

3.2 The mechanism that induces the transient growth

Due to the independence of the maximum growth of perturbations on the Reynolds number (see Figs. 4 and 7), we choose the case with $Re=2670$ and $L_z=\pi$ to further analyze the mechanism inducing the transient growth of the perturbations. Figure 8 gives the evolution of the component-wise r.m.s. with time. It can be seen that the perturbations in the wall-normal and spanwise components (v_{rms} and w_{rms}) are larger than those in streamwise component (u_{rms}) initially and that the latter rapidly increases and reaches the maximum at $t=125$ (see vertical line in Fig. 8). These results indicate transfer of energy from v_{rms} and w_{rms} to the u_{rms} during the time evolution and therefore imply that the lift-up mechanism^[4] is active.

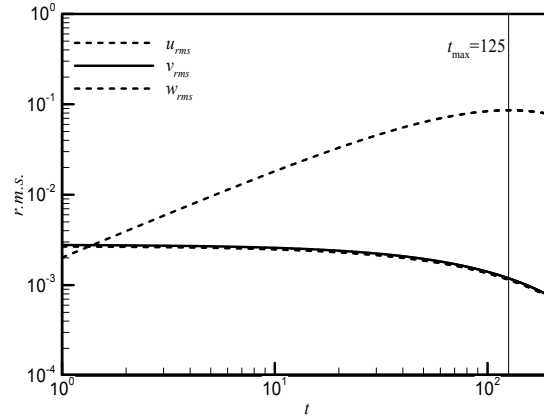


Fig. 8 Component-wise r.m.s. values when optimizing for time $t=125$.

Figure 9 shows the distributions of streamwise vortices and velocity vectors of the perturbations in y - z section at time $t=1$ and $t=125$ at the optimal initial condition. At the early period (Fig. 9(a)), there is a pair of strong positive and negative streamwise vortices alternating in z direction, due to the larger v_{rms} and w_{rms} at $t=1$ in Fig. 8. The drastic upward and downward perturbation velocities at $z=\pi(0)$ and $z=1/2\pi$, respectively, induce the perturbative motion in wall-normal direction which is the source of the lift-up mechanism. As time evolves (Fig. 9(b)), perturbation velocities in the y - z section and the corresponding streamwise vorticity decrease. The energy is extracted and transferred to the streamwise direction which leads to stronger streamwise perturbation velocity at $t=125$, as is shown in Fig. 8.

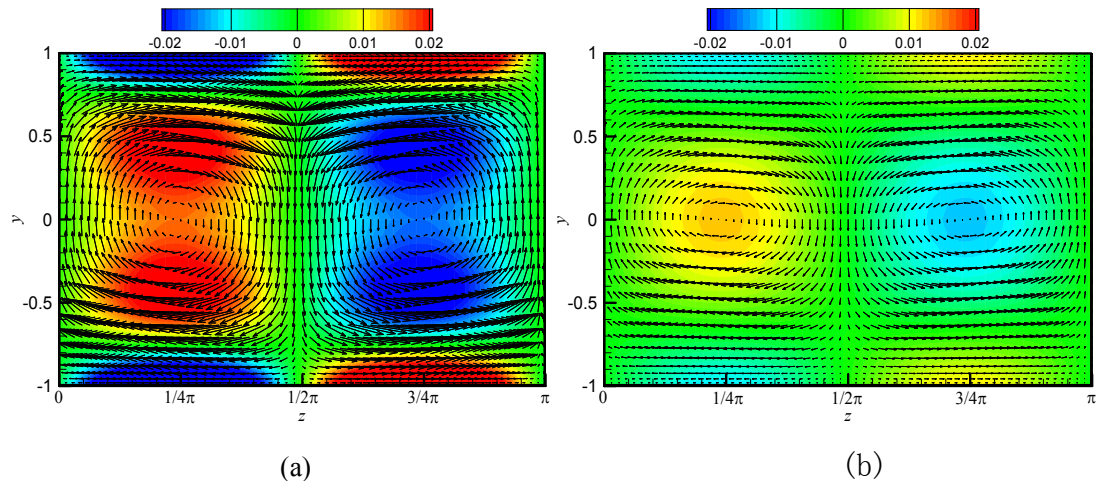


Fig. 9 Streamwise vortices (colors) and perturbation velocities (vectors) in y - z section for case with $Re=2670$ and $L_z=\pi$. (a) $t=1$, (b) $t=125$.

3.3 Validity of the algorithm

Recall that perturbation growth reaches its maximum at $\beta=2$ in Fig.7, regardless of the Reynolds number. This conclusion is consistent with the result obtained at $Re=1000$ by Reddy and Henningson^[21] and that at $Re=5000$ by Butler and Farrell^[4], both computed from the OSS equations for Poiseuille flow. To further validate the algorithm presented in this work, we compute the optimal growth at $\beta=2$ (corresponded to $L_z=\pi$) for $Re=2670$ in two other ways. One is to use the OSS equation with $\beta=2$ given. The other is to cross-check the growth of the optimal initial perturbation over time^[6] with spanwise width $L_z=\pi$. For the cross-check, the perturbation growth can be expressed as

$$\frac{E(t)}{E(0)} = \frac{\frac{1}{2} \int_{\Omega} \mathbf{u}(t) \cdot \mathbf{u}(t) d^3x}{\frac{1}{2} \int_{\Omega} \mathbf{u}(0) \cdot \mathbf{u}(0) d^3x} = \frac{\int_{\Omega} \mathbf{u}(t) \cdot \mathbf{u}(t) d^3x}{\int_{\Omega} \mathbf{u}(0) \cdot \mathbf{u}(0) d^3x} \quad (19)$$

where $\mathbf{u}(0)$ is the optimal initial perturbation and $\mathbf{u}(t)$ is the perturbation at time t , which is carried out by linearized forward DNS codes by taking $\mathbf{u}(0)$ as initial perturbation.

Figure 10 compares the optimal growth of the perturbation calculated in the three ways. It can be seen that the profile of $G(t)$ computed by our algorithm agrees well with that by the OSS equations. However, the cross-check method under-predicts $G(t)$. This is probably due to the mesh resolution of DNS. The maximum values of perturbation growth (G_{\max}) for our algorithm, the OSS method and the cross-check method are 502.4, 502.6 and 483.6, respectively. Therefore the relative error of our

result is only 0.04% compared with the OSS method. These comparisons verify the accuracy of the algorithm in this work.

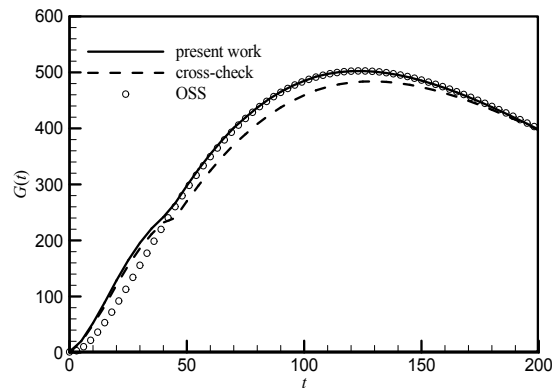


Fig. 10 Transient growth by different methods for case of $Re=2670$. The solid line is the result by present work with $L_z=\pi$, the dashed line is the result by cross-check method, and the symbol represents the result by OSS method at $\beta=2$.

It should be noted that the direct optimal growth method in this paper is suitable for complex base flows, such as $\mathbf{U}(x, y, z, t)$, to which the OSS method is not applicable. In the future work, such complex flows in channel will be employed to investigate the transient growth behaviors of the perturbations.

4 Conclusions

In this study, we improve the direct optimal growth method, which is proposed by Barkley et al.^[6], and develop an algorithm that compute the transient growth behavior of perturbations in channel flows. In this algorithm, a re-orthogonalization Anoldi method is adopted to improve the orthogonality of orthogonal basis of the Krylov subspace; the linearized adjoint NS equations are deduced to meet the specific boundary conditions of channel flow; in addition, a convergence criterion based on the residential norm of leading eigenvalue is proposed to obtain the solutions.

The algorithm is applied in the simple plane Poiseuille flow in a channel box. The effects of spanwise width of the channel and Reynolds number on transient

growth of perturbations are discussed. The largest optimal growth of perturbations is found to be at spanwise width $L_z=\pi$ for both $Re=1000$ and $Re=2670$ cases. The width corresponds to the spanwise wave number $\beta=2$ that has been observed in literatures. The optimal initial flow field shows that the structures of high- and low-speed streaks and streamwise vortices induce the lift-up mechanism and therefore lead to the transient growth of perturbations.

The algorithm is well validated by the results of the OSS equations and of the cross-check method for a plane Poiseuille flow. However, it is not limited to such flow but is suitable for any complex base flows in channel.

References

- [1] Juniper, M. P., Hanifi, A., and Theofilis, V. Modal stability theory. *Applied Mechanics Reviews*, **66**(2), 193-210 (2014)
- [2] Trefethen, L. L., Trefethen, A. E., Reddy, S. C., and Driscoll, T. A. Hydrodynamic stability without eigenvalues. *Science*, **261**, 578–584 (1993)
- [3] Schmid, P. J. Nonmodal Stability theory. *Annual Review Fluid Mechanics*, **39**,129-162 (2007)
- [4] Butler, K. M., and Farrell, B. F. Three-dimensional optimal perturbations in viscous shear flow. *Physics of Fluids A*, **4**(8), 1637-1650 (1992)
- [5] Schmid, P. J., and Henningson, D. S. *Stability and Transition in Shear Flows*. Springer, New York (2001)
- [6] Barkley, D., Blackburn, H. M., and Sherwin, S. J. Direct optimal growth analysis for timesteppers. *International Journal for Numerical Methods in Fluids*, **57**(9), 1435-1458 (2008)

- [7] Blackburn, H. M., Barkley, D., and Sherwin, S. J. Convective instability and transient growth in flow over a backward-facing step. *Journal of Fluid Mechanics*, **603**(3), 271–304 (2008)
- [8] Blackburn, H. M., Sherwin, S. J., and Barkley, D. Convective instability and transient growth in steady and pulsatile stenotic flows. *Journal of Fluid Mechanics*, **603**(9), 267–277 (2008)
- [9] Griffith, M. D., Thompson, M. C., Leweke, T., and Hourigan, K. Convective instability in steady stenotic flow: optimal transient growth and experimental observation. *Journal of Fluid Mechanics*, **655**(9), 504-514 (2010)
- [10] Mao, X., Sherwin, S. J., and Blackburn, H. M. Transient growth and bypass transition in stenotic flow with a physiological waveform. *Theoretical and Computational Fluid Dynamics*, **25**(1), 31-42 (2011)
- [11] Abdessemed, N., Sharma, A., Sherwin, S. J., and Theofilis, V. Transient growth analysis of the flow past a circular cylinder. *Physics of Fluids*, **21**(4), 044 103 (2009)
- [12] Cantwell, C. D., and Barkley, D. Computational study of subcritical response in flow past a circular cylinder. *Physical Review E*, **82**, 026315 (2010)
- [13] Mao, X., Sherwin, S. J., and Blackburn, H. M. Non-normal dynamics of time-evolving co-rotating vortex pairs. *Journal of Fluid Mechanics*, **701**(32), 430-459 (2012)
- [14] Cantwell, C. D., Barkley, D., and Blackburn, H. M. Transient growth analysis of flow through a sudden expansion in a circular pipe. *Physics of Fluids*, **22**(3), 034 101 (2010)
- [15] Sharma, A. S., Abdessemed, N., Sherwin, S. J., and Theofilis, V. Transient growth mechanisms of low Reynolds number flow over a low-pressure turbine blade, *Theoretical and Computational Fluid Dynamics*, **25**(1), 19-30 (2011)
- [16] Lehoucq, R. B., Sorensen, D. C., and Yang, C. ARPACK Users' Guide: Solution of

- Large-Scale Eigenvalue Problems with Implicitly Restarted Arnoldi Methods. *Tech. Rep.*
from <http://www.caam.rice.edu/software/ARPACK>, Computational and Applied
Mathematics, Rice University (1997)
- [17] Canuto, C., Hussaini, M. Y., Quarteroni, A., and Zang, T. A. *Spectral Methods in Fluid
Dynamics*, Springer, Berlin (1988)
- [18] Li, J., and Dong, G. Numerical simulation on evolution of subharmonic low-speed streaks in
minimal channel turbulent flow. *Applied Mathematics and Mechanics (English Edition)*,
34(9), 1069-1082 (2013)
- [19] Li, J., Dong, G., and Zhang, J. Numerical study on evolution of subharmonic varicose
low-speed streaks in turbulent channel flow. *Applied Mathematics and Mechanics (English
Edition)*, **37**(3), 325-340 (2016)
- [20] Fan, B., and Dong, G. *Principles of turbulence control*, John Wiley and Sons, Singapore
(2016)
- [21] Reddy, S. C., and Henningson, D. S. Energy growth in viscous channel flows. *J. Fluid Mech.*,
252, 209-238 (1993)